Applied Physics Letters

Phonon relaxation time reconstruction from transient thermal grating experiments and comparison with density functional theory predictions

Cite as: Appl. Phys. Lett. **114**, 023106 (2019); https://doi.org/10.1063/1.5062846
Submitted: 25 September 2018 . Accepted: 30 December 2018 . Published Online: 16 January 2019

Mojtaba Forghani, and Nicolas G. Hadjiconstantinou

Applied Physics Letters ARTICLE scitation.org/journal/apl

Phonon relaxation time reconstruction from transient thermal grating experiments and comparison with density functional theory predictions

Cite as: Appl. Phys. Lett. **114**, 023106 (2019); doi: 10.1063/1.5062846
Submitted: 25 September 2018 · Accepted: 30 December 2018 · Published Online: 16 January 2019

Mojtaba Forghani and Nicolas G. Hadjiconstantinou[a)]

AFFILIATIONS

Department of Mechanical Engineering, Massachusetts Institute of Technology, Cambridge, Massachusetts 02139, USA

[a)] Author to whom correspondence should be addressed: ngh@mit.edu

ABSTRACT

Phonon relaxation time and free path distributions are reconstructed from experimental measurements on a two-dimensional transient thermal grating and compared with density functional theory (DFT) results for silicon. The reconstruction is performed using the inverse problem formulation of Forghani *et al.* [Phys. Rev. B **94**, 155439 (2016)]. The discrepancies observed between reconstructed and DFT results are analyzed in terms of the ability of each set of data to reproduce the experimental temperature relaxation profiles; the reconstructed data are found to predict temperature profiles in closer agreement with the experimental data than the DFT results, possibly due to discrepancies between the actual material and the idealized model studied in the DFT calculations. The reconstructed phonon properties accurately predict temperature relaxation profiles at grating length scales smaller than those spanned by the experimental data. This is a very important feature since in a variety of experimental setups, including the one providing the data in the present study, measurements are not available at all scales spanned by the material free paths.

Due to the failure of Fourier's law at length scales smaller than or on the order of phonon free paths, phonon dynamics in the context of nanoscale solid-state heat transport has received considerable attention.[1–13] One area of significant interest is the extraction of phonon relaxation times and free path distribution from thermal spectroscopy experiments.[1–6] This information is crucial in a variety of applications; examples include thermal management in nano-electronic circuits and devices,[7,8] micro-electromechanical sensors,[9] and nano-structured materials for improved thermoelectric conversion efficiency.[6,10] Although density functional theory (DFT) has been widely used to predict phonon properties,[11,12] it has yet to rise to a stature level where it can replace experimental results, in part due to its failure to consistently reproduce experimental observations.[12]

In the present letter, we perform a direct comparison between DFT-derived phonon relaxation times and those reconstructed from experimentally measured temperature profiles in a two-dimensional transient thermal grating (2D-TTG) geometry.[4] The reconstruction is performed using the recently proposed inverse problem framework.[2,3] Boltzmann transport equation (BTE) solutions are provided by the adjoint deviational Monte Carlo (MC) methodology;[14–17] in other words, validity of Fourier's law is never assumed. In addition to the above comparison, we evaluate the ability of the reconstruction methodology to perform on real experimental data and under conditions where measurements are available for only a portion of the length scales spanned by material free paths; the latter is typically severely limiting for effective thermal conductivity-based methodologies.[3] Performing on real experimental data can be challenging not only due to the presence of noise but also due to other spurious signals [see Fig. 1(b)]; in addition, it tests the hypothesis, implicit in this methodology, that the experimental setup can be adequately modeled using the BTE (subject to appropriate boundary conditions).

Phonon-mediated heat transport in thermal spectroscopy experiments can be described by the linearized BTE, whose

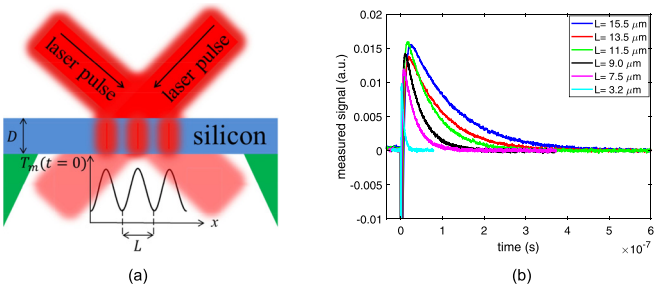

FIG. 1. (a) The 2D-TTG experiment; a sinusoidal temperature profile (T_m in the figure) with different wavelengths (L) is created at time $t = 0$ via crossing two varying angled pump pulses. A fast detector measures the combined diffracted probe light and the reference beam.[4] The Si film thickness is constant at $D = 400$ nm. (b) A few examples of the measured signal for different length scales. Nineteen wavelengths in the range of $L = 1.6$–21 μm were measured.

solution, and as a result the temperature relaxation field, is a function of the relaxation time function τ_ω (see supplementary material). Our goal is to obtain a reliable approximation to τ_ω by minimizing the discrepancy between the experimental temperature measurements and the BTE solutions. Relaxation times in the optimization formulation are represented by τ_ω^S, where ω is the phonon frequency and $S \in \{LA, TA_1, TA_2, LO, TO_1, TO_2\}$ is the branch, in which LA and LO denote the longitudinal acoustic and optical branches, respectively, TA_1 and TA_2 represent the two transverse acoustic branches, and TO_1 and TO_2 represent the two transverse optical branches, respectively. The objective function that needs to be minimized is

$$\mathcal{L} = \min_{\mathbf{U}} \left[\sum_{L,\mathbf{x},t\geq t_0} w_L |c_L S_m(t,\mathbf{x};L) - T_{BTE}(t,\mathbf{x};L,\mathbf{U})| + \alpha \left| 1 - \frac{1}{3\kappa} \int_\omega C_\omega \tau_\omega(\mathbf{U}) v_\omega^2 d\omega \right| \right], \quad (1)$$

in which L denotes the grating period [problem characteristic length scale—see Fig. 1(a)], $\mathbf{x}$ is the measurement location, $t_0 = t_0(L)$ is the first measurement time for each length scale used in the optimization, S_m is the experimentally measured signals [see Fig. 1(b)], T_{BTE} is the temperature obtained from solution of the BTE, C_ω is the frequency-dependent volumetric heat capacity, v_ω is the phonon group velocity, and w_L is a length scale dependent weight that ensures that all gratings contribute equally to the optimization; its value is given by $w_L = 1/(nN_L)$, where n is the number of different wavelengths for which data exist and N_L is the number of datapoints (in time) for each L. The objective function $\mathcal{L}$ is minimized over $\mathbf{U}$, which is the set of unknowns that the relaxation time function is parameterized with, that is, $\tau_\omega = \tau_\omega(\mathbf{U})$. Detailed expressions for $\mathbf{U}$ as well as for functional forms for the relaxation times can be found in the supplementary material. The first term in (1) ensures that the BTE solution predicts temperatures that are in agreement with the measured signals, while the second term, through a weighting factor $0.01 < \alpha < 1$, guarantees that the optimized τ_ω predicts a thermal conductivity, κ, as close as possible to the given value (presumed known). The parameter c_L that provides the optimal scaling between S_m and T_{BTE} can be calculated using a convex optimization formulation that has an analytical solution (see supplementary material).

As in our previous work,[2,3] the reconstruction is based on an optimization process utilizing the Nelder-Mead algorithm.[18] The description of the algorithm and typical parameter values can be found in Ref. 2. Details of the optimization process are provided in the supplementary material. Reconstruction proceeds by comparing solutions of the BTE, obtained via adjoint MC simulations,[17] with the counterpart $N = \sum_L N_L$ measurements of S_m.

The reconstruction method has been applied to the experimental measurements of a 2D-TTG geometry on silicon, obtained from Ref. 4. A sketch of the 2D-TTG geometry and a few examples of measured relaxation signals can be found in Fig. 1. The negative values in the signal at very early times [see Fig. 1(b)] are associated with electronic excitations that are not modeled in this work; as a result, the corresponding data are not used in the optimization process. In other words, optimization is performed over data satisfying $t > t_0(L)$ for each measurement wavelength. More details on how $t_0(L)$ is calculated can be found in the supplementary material.

In the absence of a true benchmark (actual relaxation times of material used in experiment), our reconstructed results are compared to two sets of DFT data for silicon. The first is described in Ref. 12 and will be referred to as "model A"; the second model, which features no separation in branches, was obtained using the ShengBTE DFT package[19] and will be referred to as "model B". A comparison between the DFT calculated properties and the optimization results is provided in Fig. 2; the cumulative distribution function (CDF) of free paths, denoted $F(\Lambda)$, is defined as $F(\Lambda) = \frac{1}{3\kappa}\int_{\omega^*(\Lambda)} C_\omega v_\omega^2 \tau_\omega d\omega$, where $\omega^*(\Lambda)$ is the set of modes such that $\Lambda_\omega \leq \Lambda$. Here, we recall that our reconstruction process assumes knowledge of the density of states (DOS) and group velocities (GV) and, as a result, for comparison with each of the DFT models, the corresponding DOS and GV were used. In other words, as seen in Fig. 2, two reconstructions were performed, each using the DOS and GV of the DFT model intended to be compared with and referred to using the corresponding designation. Similarly, the κ in (1) for each model is calculated based on the DOS, GV, and relaxation time function of that model.

Overall, the level of agreement between the DFT and the corresponding reconstructed data is very good, both at the relaxation time level [Figs. 2(a) and 2(b)] and at the free path CDF level [Fig. 2(c)]. However, closer examination of Fig. 2 reveals some discrepancies between each reconstructed set of data and its corresponding DFT model which could be instructive to investigate. We have eliminated the possibility that these discrepancies arise from removing the early time signal by changing the time window over which we assume that the electronic excitation part vanishes (time t_0) and observing no change in the reconstructed properties (details are provided in the supplementary material). This is expected since the electronic excitation part is a very small fraction of each signal [see Fig. 1(b)]. Another possibility is imperfect reconstruction due to the lack of measurements at all relevant length scales [the length scales used in the experiments lie in the range $1.6 \leq L \leq 21\,\mu$m, which

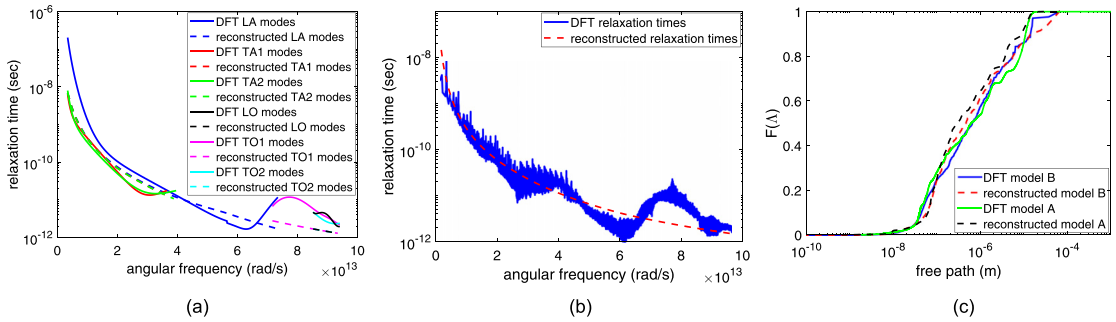

FIG. 2. Comparison between reconstructed materials properties and DFT calculations. (a) Reconstructed and "model A" DFT calculations of relaxation times. (b) Reconstructed and "model B" DFT calculations of relaxation times. (c) Reconstructed, "model A," and "model B" DFT calculation of free path distribution.

does not cover the sub-micron region (2 nm–1 μm) of the free path range of silicon (2 nm–100 μm)]. On the other hand, as discussed in Ref. 3, the reconstruction methodology used here is quite robust to such scarcity of data. This is further investigated below. A final possibility is that the DFT data do not exactly capture the experimental material behavior, most likely due to non-idealities associated with the experiment (e.g., experimental error, boundary conditions, material characterization, and purity).

In order to further investigate the above, and in the absence of a direct benchmark, we use the experimental data as a benchmark. In other words, we assess the accuracy of the reconstructed τ_ω by comparing the temperature relaxation profiles it predicts (obtained by solving the BTE using that data) to the experimental temperature profiles; we expect that the more accurate the reconstruction, the closer the temperature profiles predicted by it will be to the experimental traces. Figure 3(a) shows a comparison between the experimental traces and the DFT prediction for two wavelengths; Fig. 3(b) shows the corresponding comparison [for the same wavelengths as Fig. 3(a)] between the experimental traces and those predicted using the reconstructed τ_ω. The trends observed in Figs. 3(a) and 3(b) are representative of other wavelengths, not shown here in the interest of brevity. We first remark that the excellent match observed in Fig. 3(b) highlights the high accuracy of the reconstruction methodology used here, even in the presence of noise in both measurements and MC simulations, as well as the presence of other spurious signals (electronic excitation). A comparison between the two figures also reveals that the discrepancies are clearly smaller in the case of the reconstructed τ_ω; this implies that most of the discrepancy between the reconstructed and DFT data is likely due to differences between the idealized (DFT) and real (experimental) material behavior.

As noted above, the reconstruction method used here is able to accurately reconstruct materials properties even at length scales for which no experimental measurements exist (see supplementary material for additional discussion). This is demonstrated in Fig. 3(c), which compares the relaxation profile as predicted by the reconstructed and DFT data for L = 500 nm and 200 nm (which is significantly smaller than the smallest length scale for which experimental data were available, L = 1.6 μ m). The overall agreement is very good; an analysis of the sensitivity of this reconstruction to each optimization parameter can be found in the supplementary material. We do note, however, that in the "small-L" regime, transport becomes increasingly ballistic and thus less sensitive to relaxation times. We therefore performed a second numerical experiment to ensure that the above assertion is indeed true.

In this second experiment, we performed the reconstruction using a subset of the available experimental data (10 μm $\leq$ L $\leq$ 21 μm) and used some of the remaining data (L = 1.8 μm and L = 2.4 μm) for comparison with our predictions. The results are shown in Fig. 4 (for a sensitivity

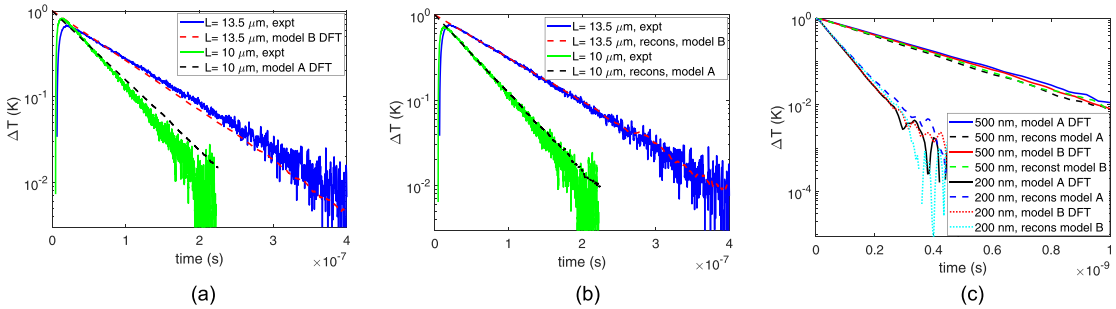

FIG. 3. Comparison between experimentally measured ("expt"), reconstructed ("recons"), and DFT-based simulated temperature profiles. (a) DFT vs. experimental measurements. (b) Reconstructed vs. experimental measurements. (c) DFT vs. reconstructed for the sub-micron regime. All "recons" results are based on reconstructions of Fig. 2.

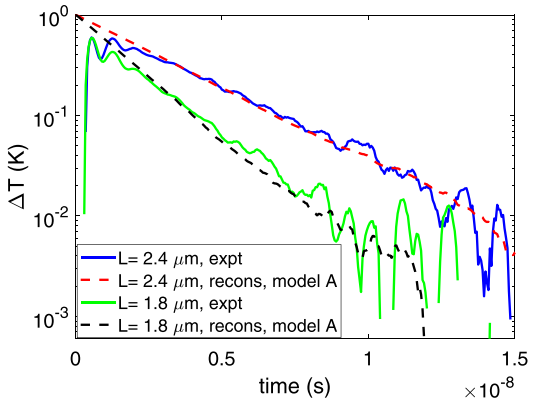

FIG. 4. Comparison between experimentally measured ("expt") temperature relaxation profiles and those predicted by reconstructed data ("recons") using information on experiments in the range $L = 10$–$21\ \mu$m.

analysis, see supplementary material). The good agreement between measured and simulated temperatures [after t_0 ($1.8\ \mu$m) = 2.3 ns and t_0 ($2.4\ \mu$m) = 2.8 ns] shows that the reconstruction method used here provides reliable predictions even for length scale regimes not represented in the experimental data. This is due to the fact that this method retains a spectral parametrization of phonon properties. This is in sharp contrast to effective thermal conductivity-based approaches which project the information about the experimental data onto a few-parameter model of the process (e.g., an exponential response with an effective thermal conductivity/diffusivity), thereby significantly reducing its information content, while introducing error (Fourier-like behavior is only valid for sufficiently large length scales and late times[2]). This reduction in information content aggravates the ill-posedness of the reconstruction, requiring intervention, such as imposition of smoothness requirements,[5] to avoid unphysical solutions (see Ref. 3 for a longer discussion).

In summary, in this letter, we have shown that the framework proposed in Ref. 2 can be reliably used to reconstruct from experimental data, where non-idealities (e.g., noise or other spurious signals) as well as modeling discrepancies (e.g., boundary effects) make reconstruction challenging. In the case of silicon studied here, the reconstructed results were found to be in overall good agreement with DFT results. Small discrepancies were shown to be primarily due to the inability of DFT to precisely capture the experimental material behavior, most likely due to effects present in the experiment not captured by the idealized material studied within the DFT model. The sensitivity analysis detailed in the supplementary material provides a tool for *a posteriori* identification of elements of **U** to which the objective function is relatively insensitive and which, as a result, may not be accurately determined. These considerations make reconstruction methodologies uniquely positioned as a reliable complement to DFT calculations.

See supplementary material for more information on transport modeling, optimization formulation, and sensitivity analysis.

The authors would like to thank S. C. Huberman for providing the "model B" DFT data, A. A. Maznev for providing the experimental measurements, and the anonymous referee for suggesting the sensitivity analysis included in the supplementary material. This work was supported by the Solid-State Solar-Thermal Energy Conversion Center (S3TEC), an Energy Frontier Research Center funded by the U.S. Department of Energy, Office of Science, Basic Energy Sciences, under Award No. DE-SC0001299 and DE-FG02-09ER46577.

REFERENCES

[1]A. J. Minnich, J. A. Johnson, A. J. Schmidt, K. Esfarjani, M. S. Dresselhaus, K. A. Nelson, and G. Chen, Phys. Rev. Lett. **107**, 095901 (2011).
[2]M. Forghani, N. G. Hadjiconstantinou, and J.-P. M. Péraud, Phys. Rev. B **94**, 155439 (2016).
[3]M. Forghani and N. G. Hadjiconstantinou, Phys. Rev. B **97**, 195440 (2018).
[4]J. A. Johnson, A. A. Maznev, J. Cuffe, J. K. Eliason, A. J. Minnich, T. Kehoe, C. M. Sotomayor Torres, G. Chen, and K. A. Nelson, Phys. Rev. Lett. **110**, 025901 (2013).
[5]A. J. Minnich, Phys. Rev. Lett. **109**, 205901 (2012).
[6]M. Zebarjadi, K. Esfarjani, M. S. Dresselhaus, Z. F. Ren, and G. Chen, Energy Environ. Sci. **5**, 5147–5162 (2012).
[7]D. G. Cahill, K. Goodson, and A. Majumdar, J. Heat Transfer **124**, 223–241 (2002).
[8]E. Pop, Nano Res. **3**, 147–169 (2010).
[9]D. G. Cahill, P. V. Braun, G. Chen, D. R. Clarke, S. Fan, K. E. Goodson, P. Keblinski, W. P. King, G. D. Mahan, A. Majumdar, H. J. Maris, S. R. Phillpot, E. Pop, and L. Shi, Appl. Phys. Rev. **1**, 011305 (2014).
[10]Z. Tian, S. Lee, and G. Chen, J. Heat Transfer **135**, 061605 (2013).
[11]A. Ward and D. A. Broido, Phys. Rev. B **81**, 085205 (2010).
[12]K. Esfarjani, G. Chen, and H. T. Stokes, Phys. Rev. B **84**, 085204 (2011).
[13]E. Pop, S. Sinha, and K. E. Goodson, Proc. IEEE **94**, 1587–1601 (2006).
[14]J.-P. M. Péraud and N. G. Hadjiconstantinou, Phys. Rev. B **84**, 205331 (2011).
[15]J.-P. M. Péraud and N. G. Hadjiconstantinou, Appl. Phys. Lett. **101**, 153114 (2012).
[16]J.-P. M. Péraud, C. D. Landon, and N. G. Hadjiconstantinou, Annu. Rev. Heat Transfer **17**, 205–265 (2014).
[17]J.-P. M. Péraud and N. G. Hadjiconstantinou, Phys. Rev. B **91**, 235321 (2015).
[18]J. A. Nelder and R. Mead, Comput. J. **7**, 308–313 (1965).
[19]W. Li, J. Carrete, N. A. Katcho, and N. Mingo, Comput. Phys. Commun. **185**, 1747–1758 (2014).